AIAA JOURNAL
Vol. 36, No. 7, July 1998

Quantitative Imaging in Proper Orthogonal Decomposition of Flow Past a Delta Wing

K. M. Cipolla,* A. Liakopoulos,† and D. O. Rockwell‡
Lehigh University, Bethlehem, Pennsylvania 18015

Snapshot proper orthogonal decomposition is used to characterize the unsteady flow past a delta wing, focusing on the structure of the leading-edge vortices. The decomposition is applied to two-dimensional velocity fields obtained via a laser-scanning version of high-image-density particle image velocimetry to extract the most coherent structures in the flow. Data are analyzed for cases involving both a stationary wing and a wing undergoing harmonic oscillations in roll. In each case, the velocity fields are reconstructed as a truncated series expansion in terms of the computed eigenfunctions from which the corresponding contours of constant vorticity and sectional streamline patterns are calculated. Comparison with the original data demonstrates that the analysis provides an accurate representation of the velocity fields while eliminating extraneous small-scale features. Inclusion of as few as two eigenfunctions in the reconstruction series reproduces the largest-scale features of the leading-edge vortices, whereas the inclusion of half of the total number of eigenfunctions produces a reconstructed field that captures the majority of the flow features. By appropriately combining the spatial and temporal components of the proper orthogonal decomposition analysis, one obtains the dynamical structures that evolve in both space and time, such as the fluctuations in the location of vortex breakdown.

Nomenclature

a_k = modal amplitudes for velocity
b = span
C = correlation matrix
c_o = centerline chord
d_I = interrogation window size
E = mean total fluctuation energy
M = total number of snapshots
N = number of modes retained in Eq. (4)
T = period of oscillation
t = time
U_∞ = freestream velocity
u = x component of velocity
$\boldsymbol{V}$ = velocity vector
v = y component of velocity
x_{vb} = location of vortex breakdown, measured along wing centerline from apex
x, y = coordinates
α_k = kth eigenvector of the correlation matrix
Δt = time interval between snapshots
κ = reduced frequency, $(\pi b)/2U_\infty T$
λ_k = kth eigenvalue of the correlation matrix
Φ = roll angle
ϕ_k = kth empirical velocity eigenfunction
$\bar{}$ = time-averaged quantities
$'$ = fluctuation quantities

I. Introduction

In recent years, increased maneuverability of swept wing aircraft has become a major priority. Maneuvers often occur at high angles of attack and with rapid changes in incidence and direction, resulting in flows that are generally unsteady and severely separated. Flight dynamics teams that are responsible for specifying and characterizing these maneuvers require detailed insight into the flow physics associated with such conditions. One important issue in considering this problem is the susceptibility to instabilities in the rolling mode. Representative experimental investigations of the general flow characteristics and the possible instabilities are those of Hanff and Jenkins,[1] Hanff and Huang,[2] and Ericsson and Hanff.[3,4] Several studies, including those by Jenkins and Myatt[5] and Jenkins et al.,[6] have been devoted to developing nonlinear models for the aerodynamic loading of delta wings based on the results of these experimental investigations.

Because the leading-edge vortices are the fundamental flow structures on a delta wing, knowledge of their behavior and inherent instabilities is necessary if methods of altering and controlling the flow are to be developed. At large angles of attack, vortex breakdown occurs over the surface of the wing, and a region of stalled flow associated with a loss of lift results. If the delta wing is at a nonzero roll angle, for either static or dynamic conditions, the complexity of the problem increases. To date, an adequate description of the alterations of the leading-edge vortex structure with variations in roll angle has not been provided.

Quantitative imaging of entire planes of the complex flowfield on a delta wing has been employed recently to reveal the physics associated with the onset and development of vortex breakdown, which traditionally has been visualized by smoke and dye injection. Magness et al.[7,8] characterized the instantaneous streamline topology and vorticity distribution in crossflow planes of a delta wing pitching with large-amplitude motion to high angle of attack. These investigations, as well as subsequent ones in recent years, show that both the instantaneous and averaged streamline topology over a cross section of the leading-edge vortex can be interpreted and classified with the aid of critical point theory. In addition, imaging in streamwise planes aligned with the axis of the leading-edge vortex, i.e., planes approximately orthogonal to crossflow planes, has allowed detailed characterization of the instantaneous structure of vortex breakdown, more specifically, the instantaneous streamline topology and contours of azimuthal vorticity. This approach has provided new insight into the physics associated with the onset of vortex breakdown and its variation with time, as described by Towfighi and Rockwell[9] and Lin and Rockwell.[10] For both of the foregoing types of characterization of the flow, i.e., the instantaneous structure in the chordwise and crossflow planes, a very

Received Jan. 30, 1998; revision received March 23, 1998; accepted for publication March 23, 1998.

*Graduate Research Assistant, Department of Mechanical Engineering and Mechanics; currently Mechanical Engineer, Submarine Sonar Department, Towed and Deployed Sensors Division, Code 2141, U.S. Naval Undersea Warfare Center, 1176 Howell Street, Newport, RI 02841. Member AIAA.

†Associate Professor, Department of Mechanical Engineering and Mechanics, 354 Packard Laboratory, 19 Memorial Drive.

‡Paul B. Reinhold Professor, Department of Mechanical Engineering and Mechanics, 354 Packard Laboratory, 19 Memorial Drive. Member AIAA.

large number of images is required to specify the features of the flow, which is inherently unsteady, either with or without imposed maneuvers of the wing. It is therefore desirable to formulate an approach that describes the key features of the flow with a minimum number of images. Moreover, recent interest in controlling these types of flows via various types of actuators invites the possibility of using global, quantitative images not only to determine the overall response to imposed control but also as a global detector for triggering the actuator, in contrast to pointwise velocity, pressure, or shear stress detectors. Again, use of a limited number of images will be essential. Detailed measurements of the two-dimensional fields of a delta wing have demonstrated the effectiveness of local control, such as fluid injection[11] and low-amplitude oscillations of the surface,[12] in altering the structure of the leading-edge vortices.

Efforts to formulate low-order models of the unsteady, complex behavior of leading-edge vortices on delta wings will require application of proper orthogonal decomposition (POD) (Ref. 13) to provide highly comprehensive image representations. In fact, as will be demonstrated herein, the technique of POD does allow faithful reconstruction of the central features of the streamline topology and vorticity fields with a limited number of modes, i.e., images, thereby demonstrating promise for broader application to aerodynamic flows. Furthermore, POD-based dynamic flow models offer a number of advantages over conventional mathematical descriptions of unsteady flows. The partial differential equations governing the dynamics of the flow can be transformed into systems of ordinary differential equations by well-established procedures. Weighted residuals methods, for example, have been successfully used in conjunction with a variety of basis functions, such as trigonometric functions, orthogonal polynomials, and splines.[14] In practice, the infinite dimensional representation is truncated to a finite n-dimensional system. To ensure that the dynamical behavior described by the resulting finite dimensional system corresponds to that of the full problem, the required dimension n is high. However, a large reduction in n is required for the development of useful low-order models. Because of its ability to compress dynamical information, POD offers a procedure for obtaining a set of optimal basis functions[15] for the weighted residuals method. POD-weighted-residuals models offer a compact description of the system dynamics, and they are potentially useful in designing, simulating, and testing flow control systems, as discussed by Berkooz et al.[15] and Liakopoulos et al.[16]

Although POD has many potential applications in fluid dynamics, extensive use of the technique has been limited by a lack of sufficient data required to perform the decomposition. The recent availability of results from computational fluid dynamics simulations has made possible the application of POD to various flow configurations, e.g., channel flow[17,18] and flat plate boundary layers.[19] From an experimental perspective, the instantaneous two-dimensional velocity fields attainable with particle image velocimetry (PIV) seem a natural complement to POD, as explored by Huang[20] for the case of flow past a backward-facing step. When the decomposition is obtained from a sequence of instantaneous spatial fields acquired at different times, the method is termed *snapshot POD*. This form of POD, introduced by Sirovich,[21] is particularly advantageous for decomposing large data sets arising in high-spatial-resolution computational or experimental studies.

In the present study, the method of snapshot POD is applied to velocity data obtained via PIV for the flow past a delta wing. Data acquired in planes oriented perpendicular to the centerline of the wing and coincident with the axes of the leading-edge vortices are considered. The overall goal of this investigation is to discern the coherent structures in the flow and thereby characterize the structure of the leading-edge vortices on a delta wing both upstream and downstream of vortex breakdown.

II. Experimental System and Techniques

Experiments were performed in a large, open-surface water channel, with a test section approximately 1 m wide × 0.5 m deep. The flow speed was 17.8 cm/s, corresponding to a Reynolds number based on the centerline chord of the wing of 3.24×10^4. The

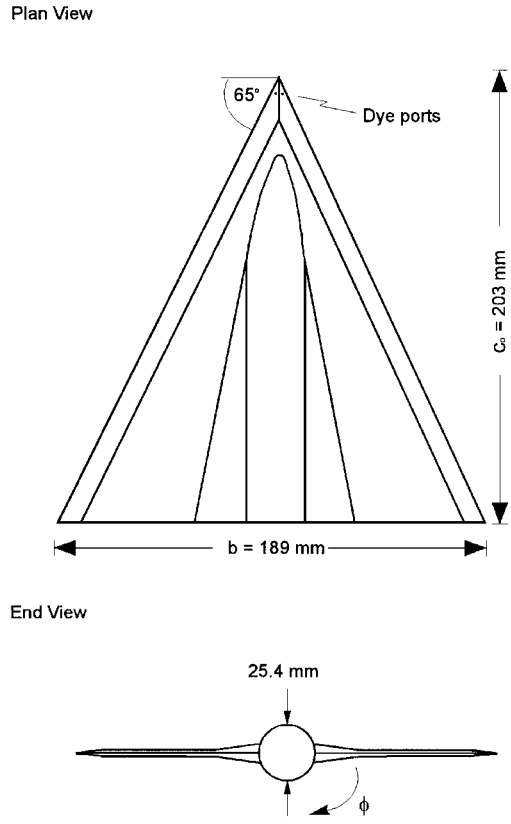

Fig. 1 Delta wing geometry.

delta wing had a sweep angle of 65 deg and a centerline chord $c_o = 203$ mm, as shown in Fig. 1. The wing is held on a long sting oriented at 30 deg to the freestream and driven by a computer-controlled motor that allows the wing to be moved to any value of roll angle (Fig. 2). The zero-roll-angle condition is established as the position where the locations of leading-edge vortex breakdown are symmetric and corresponds to a position approximately 2 deg from the vertical. This condition ensures the elimination of any effects due to asymmetries in the freestream flow. Dye injected at the apex of the delta wing (Fig. 1) marks the leading-edge vortex and enables tracking of the vortex breakdown position. Images were acquired with a 35-mm camera after the flow had reached a quasi-steady state. The camera looks into an oscillating mirror and through a water-filled Plexiglas® prism (Fig. 2) to eliminate the effects of reverse flow and light refraction, respectively. A more detailed description of the experiments is given in Ref. 22.

The instantaneous velocity fields over an entire plane of the flow were obtained via a laser-scanning version of PIV, as described by Rockwell et al.[23] A multi-faceted (72) mirror rotates at 8.7 Hz to produce a 1-mm-thick laser sheet at an effective scanning rate of 626 Hz. For the crossflow planes, the laser sheet was oriented perpendicular to the centerline of the delta wing at a location $0.10c_o$ upstream of the trailing edge. The rotating mirror is mounted on a circular disk beneath the water channel to enable adjustment of the laser sheet to an orientation coincident with the axes of the leading-edge vortices.

The images obtained as 35-mm film negatives were interrogated by a program that uses a single-frame, cross-correlation method involving the application of two successive fast Fourier transforms.[24] A typical window size $d_I \times d_I$ of 0.72×0.72 mm was used with a 50% overlap, thereby satisfying the Nyquist criterion; i.e., the step size Δl of the interrogation process did not exceed $0.5d_I$. The resulting grid size on the film was 0.36×0.36 mm, corresponding to 2.25×2.25 mm in the physical plane, with the magnification of the lens equal to 0.17.

Because standard 35-mm film was used to record the data, the number of consecutive images possible is limited to the length of a single roll of film, e.g., 36 images. This value, along with the time interval between consecutive images Δt, dictates the length

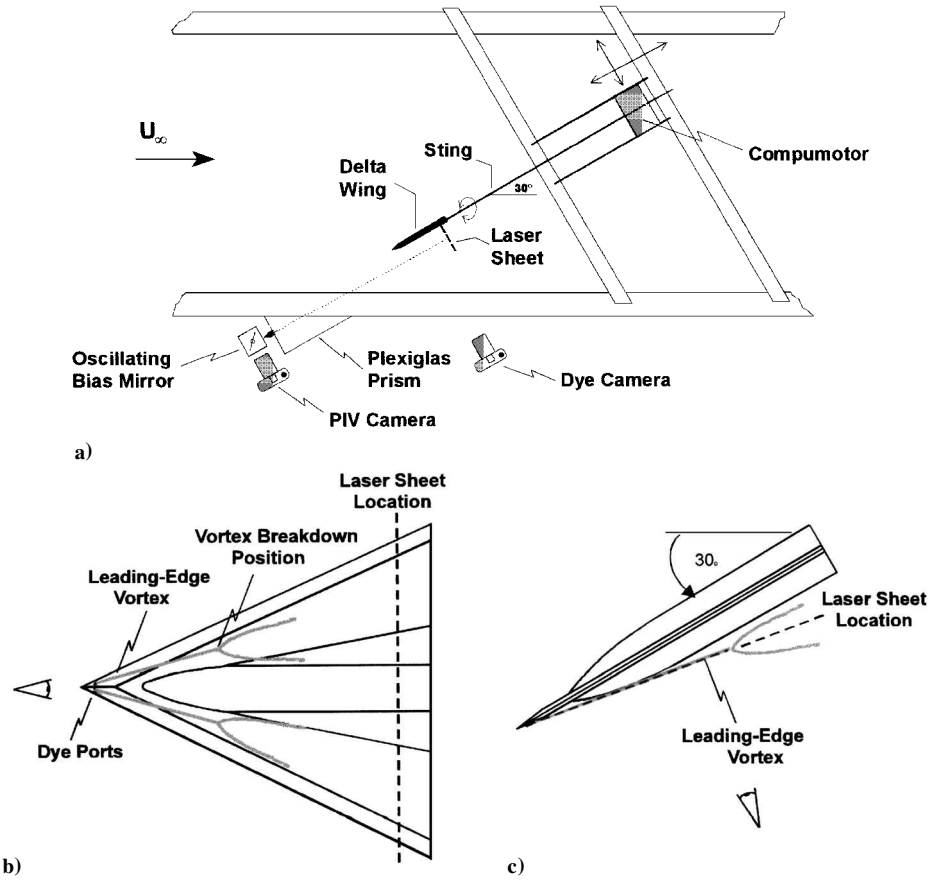

Fig. 2 Schematic of experimental setup showing a) plan view of water channel and the orientation of the laser sheet for b) crossflow data planes and c) data planes coincident with the core of the leading-edge vortex.

of the data record attainable with this experimental system. At the fastest reliable framing rate of the present camera, 2 frames/s, the maximum record length is 18 s, which is suitable for the periods of oscillation considered in this work. When the flow structure past a stationary delta wing is of interest, a Δt is chosen that is an order of magnitude larger than the convective timescale c_o/U_∞, resulting in a total record length of $210c_o/U_\infty$.

III. Basic Methodology

In the present analysis, the time-dependent velocity data acquired via PIV are separated into time-averaged and time-fluctuating components:

$$\boldsymbol{V}(x, y, t) = \bar{\boldsymbol{V}}(x, y) + \boldsymbol{V}'(x, y, t) \tag{1}$$

In Eq. (1), the time-averaged component is the ensemble average of M snapshots of the velocity field. The POD then is applied to the fluctuating component of velocity. The implementation of snapshot POD is discussed in Ref. 25 and briefly summarized in the following.

The empirical eigenfunctions $\{\phi_k,\ k = 1, 2, \ldots, M\}$ are constructed by linearly combining the time-fluctuating components of the instantaneous velocity fields:

$$\phi_k(x, y) = \sum_{m=1}^{M} \alpha_{km} \boldsymbol{V}'^m(x, y, t_m) \tag{2}$$

where $\boldsymbol{V}'^m$ denotes the mth snapshot of the fluctuating velocity field and α_k denotes the kth eigenvector of the algebraic eigenvalue problem

$$C\boldsymbol{\alpha} = \lambda\boldsymbol{\alpha} \tag{3}$$

Here, the elements of the $M \times M$ matrix C are $C_{mn} = (1/M)(\boldsymbol{V}'^m, \boldsymbol{V}'^n)$, where

$$(\boldsymbol{V}'^m, \boldsymbol{V}'^n) = \iint \boldsymbol{V}'^m(x, y, t_m) \cdot \boldsymbol{V}'^n(x, y, t_n)\, \mathrm{d}x\, \mathrm{d}y$$

Note that the matrix C is symmetric and positive semidefinite. Consequently, all eigenvalues are real and nonnegative and can be ordered such that $\lambda_1 \geq \lambda_2 \geq \lambda_3 \geq \cdots \geq \lambda_M$. Each eigenvalue represents the contribution of the corresponding eigenmode to the mean of the total fluctuation energy[21]

$$E = \iint (u'^2 + v'^2)\, \mathrm{d}x\, \mathrm{d}y = \sum_{k=1}^{M} \lambda_k$$

Therefore, this decomposition offers an objective method for the identification of the most energetic eigenfunctions, ϕ_i, $i = 1, 2, \ldots, N$, where N is problem dependent. The eigenfunctions are orthogonal to each other, and when normalized properly, i.e., $\phi_i \rightarrow \phi_i/\sqrt{\lambda_i}$, they form an orthonormal basis.

Having constructed the empirical eigenfunctions for the problem at hand, the time-fluctuating component of the velocity field can be approximated by a truncated expansion of the form

$$\boldsymbol{V}'(x, y, t) = \sum_{k=1}^{N} a_k(t)\phi_k(x, y) \tag{4}$$

where the modal amplitudes a_k are time dependent and $N \leq M$. By making use of the orthonormality of the eigenfunctions, we obtain from Eq. (4) that

$$a_k(t) = \iint \boldsymbol{V}'(x, y, t) \cdot \phi_k(x, y)\, \mathrm{d}x\, \mathrm{d}y \tag{5}$$

Finally, the original velocity field is reconstructed by applying

$$\boldsymbol{V}(x, y, t) = \bar{\boldsymbol{V}}(x, y) + \sum_{k=1}^{N} a_k(t)\phi_k(x, y) \tag{6}$$

IV. Results and Discussion

In this investigation, POD is applied to several sets of data obtained via PIV to ascertain the ability of POD to represent the time-dependent, coherent structures in the physical flowfield. First, the crossflow structure past a stationary delta wing will be considered. In this case, the leading-edge vortex structure is fairly coherent,

and the feasibility of obtaining a reasonable decomposition from a limited number of snapshots is demonstrated. Next, the flow past a stationary delta wing will be considered in terms of the structure in a plane through the axis of the leading-edge vortices. The goal of this analysis is to employ POD to provide insight into the inherent temporal fluctuations in the flow structure. Finally, a POD analysis is performed on a set of data consisting of the flow structure past a harmonically oscillating wing in crossflow planes to demonstrate quantitatively the existence of a pervasive, coherent structure throughout the motion cycle. In this case, the addition of external forcing imposes a degree of organization to the system when compared with results obtained for a stationary delta wing. The correlation of the frequency of the dominant motion and its subharmonics with flow structures of different time and length scales is addressed.

Crossflow Structure of Coherent Leading-Edge Vortex Past a Stationary Delta Wing

POD is applied to PIV data obtained in a crossflow plane to extract the most dominant features of the leading-edge vortex at a location upstream of breakdown. A sequence of 12 snapshots is decomposed using the method described in Sec. III. This set of data, although acquired when the wing is stationary and the flow has reached equilibrium, exhibits inherent fluctuations in the flow structure. The time interval between consecutive snapshots is 20 s, corresponding to $\Delta t U_\infty / c_o = 17.5$. The length of time over which the entire data record was obtained corresponds to $\Delta t U_\infty / c_o = 210$.

The normalized eigenvalues and their cumulative contributions to the velocity fluctuation energy were calculated and normalized by enforcing the condition

$$\sum_{m=1}^{M} \lambda_m = 1$$

(Ref. 22). The magnitude of the eigenvalues was found to decrease with increasing mode number, representing the decreasing contribution of the high-order modes to the total flow fluctuation energy. However, the energy is distributed over the majority of the modes rather than being concentrated in only the first few modes; 75% of the total fluctuation energy is contained in the first six modes.

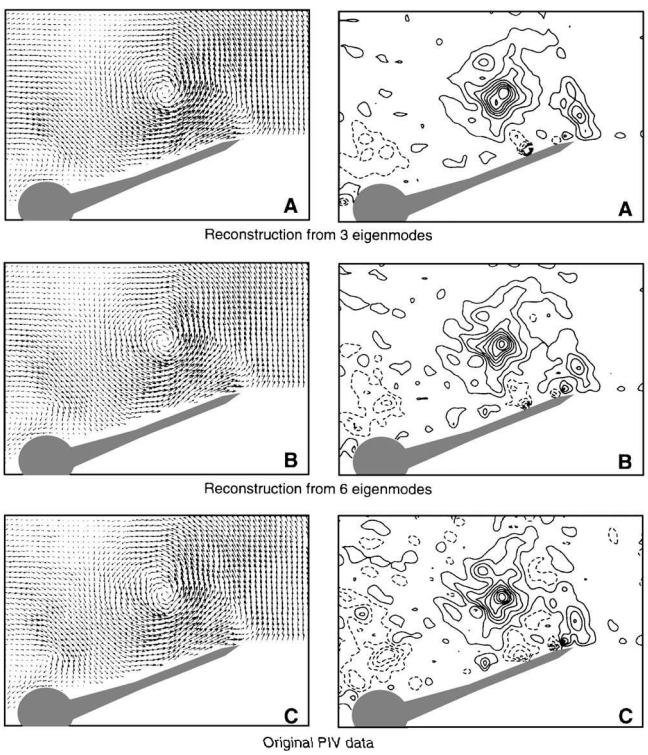

Fig. 3 Comparison of reconstructed velocity fields and patterns of vorticity with corresponding original PIV data in a crossflow plane, $\Phi = -20$ deg. Minimum and incremental vorticity levels are $\omega_{\min} = \pm 5\ s^{-1}$ and $\Delta\omega = 10\ s^{-1}$, respectively.

The reconstructed velocity field from the first three eigenmodes (A) and the first six eigenmodes (B) are compared with the corresponding original field (C) for one typical snapshot in the left-hand column of Fig. 3. The right-hand column contains the vorticity fields calculated from the adjacent velocity fields. In each image, the cross section of the wing is shown in gray, and flow is out of the page. Contours of positive (counterclockwise) and negative (clockwise) vorticity are indicated by solid and dashed lines, respectively. Inspection of image A, which captures 48.8% of the fluctuation energy, shows the dominant primary vortex and a smaller, opposite-sign vortical structure in the lower-left-hand corner of the image. In fact, the structure of the reconstructed primary vortex is a remarkably faithful representation of that in the original image C. Only a few small-scale features of the flow are reconstructed, however, as indicated by the corresponding vorticity field. Including six eigenmodes (B) in the reconstruction does not alter the velocity field substantially; however, more smaller-scale structures emerge in the vorticity field. In particular, the shape of the primary vortical structure and the extension of the shear layer that separates from the leading edge into the primary vortex more closely resembles the original data (C), displaying more irregularities in the contours than were observed in image A. Also, the concentration of negative vorticity located beneath the primary vortex that corresponds to eruption of the flow from the surface of the wing is reproduced more accurately when six modes are included, demonstrating that it is a lower-energy phenomenon than the primary vortex.

This application of snapshot POD to a sequence of PIV images demonstrates that even a limited number of snapshots can be used to produce a reasonable representation of the original data. Because the primary vortex dominates this flow and its form is fairly consistent from image to image, the fundamental flow structure is reproduced by a reconstruction based on three eigenmodes only. Structures that are smaller and weaker than the primary vortex, such as the separation of the boundary layer at the surface, are revealed more clearly when half of the calculated modes are included in the reconstruction. This representation captures 75% of the fluctuation energy.

Time-Dependent Fluctuations in the Structure of the Leading-Edge Vortices

The preceding section explored the possibility of applying POD to a very limited number of snapshots; fairly good results were obtained. In this section, POD is performed on a larger sample with a much higher time resolution to study the time-dependent fluctuations of the location of leading-edge vortex breakdown. The complete sequence of images consists of 33 snapshots, i.e., $M = 33$, acquired in a plane through the core of the leading-edge vortices at 0.5-s time intervals.

As in the preceding analysis, the normalized eigenvalues and their cumulative sums were calculated.[22] Inspection of the results showed that the largest eigenvalues occur in pairs of comparable magnitude; a similar pairing was observed by Sahan et al.[25] Also, it was found that approximately 75% of the total fluctuation energy is accumulated in the first 15 of the computed eigenmodes. The corresponding gradual decline in the magnitude of the eigenvalues indicates that a large number of structures of varying scale and fluctuation energy exist in the flow.

Several eigenfunctions for the fluctuating component of velocity are shown in Fig. 4. The first three modes, corresponding to normalized eigenvalues of 0.152, 0.111, and 0.0679, respectively, contain the large-scale features of the fluctuating velocity field, although some smaller-scale structures are apparent in the plots of the second and third eigenmodes. In the fifth eigenmode, which captures 4.9% of the fluctuation energy, only features whose characteristic lengths are an order of magnitude smaller than the chord length are captured. The 10th and 15th eigenmodes correspond to normalized eigenvalues of 0.0294 and 0.0229 and are composed of features that are five times smaller in energy level than those in the first 2 eigenmodes. Higher-order modes are not included in the reconstruction because the computed high-order eigenfunctions typically are less accurate.

Figure 5 contains the velocity fields (left-hand column) and the patterns of vorticity (right-hand column) for one representative instant. The reconstructed fields based on 2 eigenmodes (A) and 15

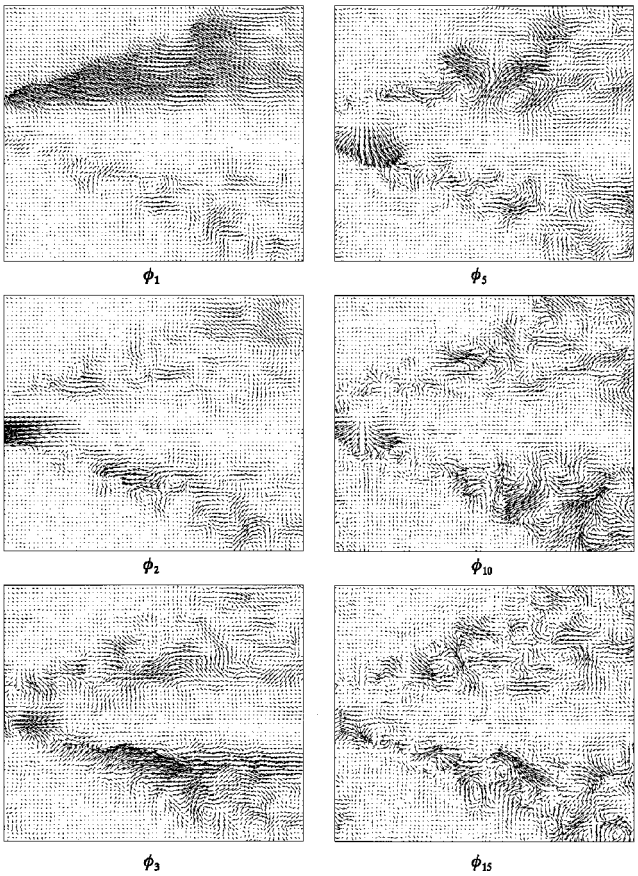

Fig. 4 Representative eigenfunctions for the fluctuating component of velocity.

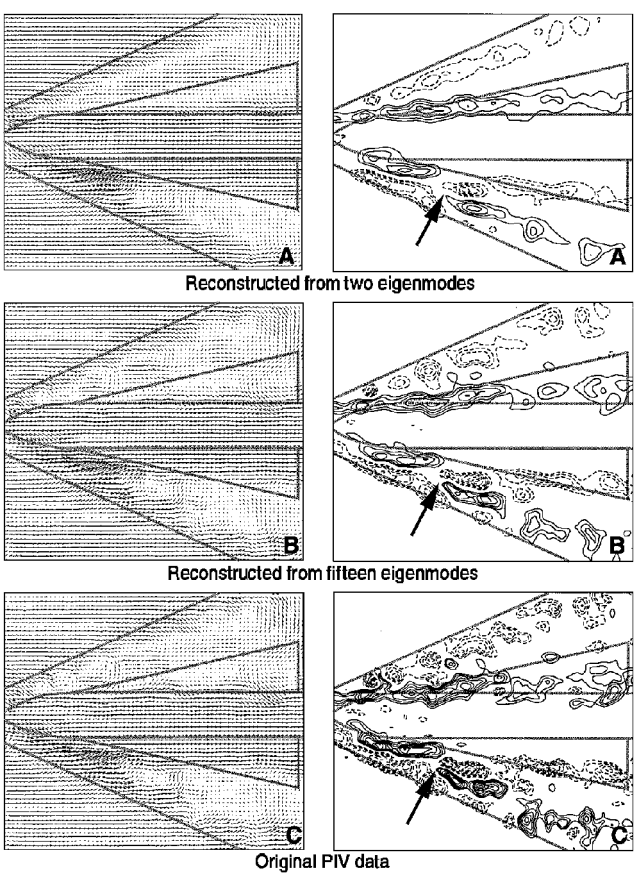

Fig. 5 Instantaneous velocity fields and patterns of vorticity for one representative instant; plane of observation is coincident with axis of vortex. Minimum and incremental vorticity levels are $\omega_{min} = \pm 10\,s^{-1}$ and $\Delta\omega = 5\,s^{-1}$, respectively; $\Phi = 4$ deg.

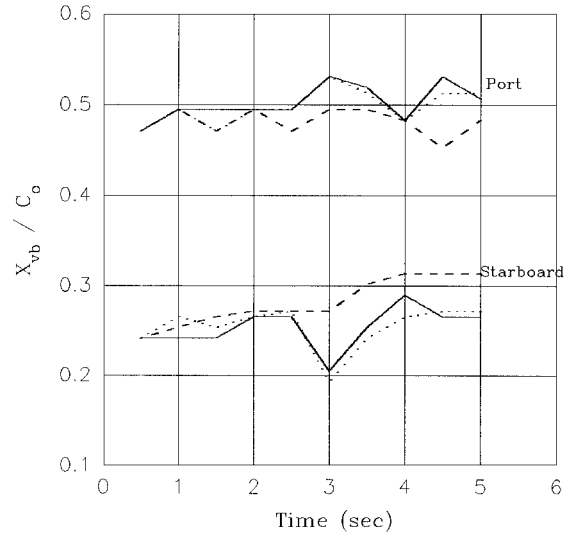

Fig. 6 Location of vortex breakdown x_{vb}/c_o of the port and starboard leading-edge vortices vs time for PIV data (——) and data reconstructed from 2 (– – –) and 15 (· · · ·) eigenmodes.

eigenmodes (B) are shown above the corresponding original fields (C). The location of the delta wing, which lies outside of the laser sheet, is projected onto the field of view and shown as an outline in each image. The mean flow is from left to right. Although the large-scale, leading-edge vortex structure is apparent in the low-order reconstruction in the top pair of images (A), which captures 26% of the fluctuation energy, the smaller-scale, discrete structures in the breakdown (downstream) region are lost. The switch in the sign of vorticity, indicating the location of vortex breakdown,[9] is marked by an arrow in each vorticity field in Fig. 5. Its existence in the low-order reconstruction (A) at a spatial location corresponding to that in the original data (C) verifies that vortex breakdown is a high-energy phenomenon that dominates the flow. In contrast, the majority of the important smaller-scale features are reproduced by retaining the first 15 eigenmodes, which represent 75% of the energy, in the reconstruction (B). Individual concentrations of vorticity emerge downstream of vortex breakdown, as observed in the original data field (C). Finally, note that truncating the reconstruction series at 15 terms [Eq. (6) with $N = 15$] eliminates some of the smallest-scale features that exist in the original data.

The loss of the smaller-scale flow features in the two-eigenmode reconstruction is further illustrated by considering the variation in the location of vortex breakdown in consecutive snapshots. Figure 6 is a plot of the dimensionless location of breakdown x_{vb}/c_o of the port and starboard leading-edge vortices in the first 10 images in the time sequence; it compares results from reconstructions employing 2 eigenmodes and 15 eigenmodes to those from the original PIV data. The values of x_{vb}/c_o correspond to the locations (designated by arrows in Fig. 5) at which a switch in the sign of vorticity occurs in the patterns of contours of constant vorticity. Although the values obtained from the 15-eigenmode reconstruction (dotted line) follow the curve from the original data (solid line) quite closely, it is obvious that the 2-eigenmode reconstruction (dashed line) has not captured the small-scale fluctuations of the location of breakdown observed in the experimental data.

Consideration of the modal amplitudes $\{a_k\}$ provides insight into the different timescales inherent to the flow structure. These expansion coefficients $a_k(t)$ are determined by direct projection of the snapshots on the computed eigenfunctions [Eq. (5)] and are plotted in Fig. 7 for the most energetic modes, $k = 1, 2, \ldots, 7$. The first expansion coefficient $a_1(t)$ represents a low-frequency flow mechanism that does not exhibit any particular periodicity within the sampling time of the original data. The second and third modal amplitudes, $a_2(t)$ and $a_3(t)$, reflect higher frequencies associated with the smaller-scale spatial structures observed in the second and third eigenfunctions. Similar frequencies and amplitudes are seen in the fourth and fifth modal amplitudes. However, temporal modes six and seven display even higher frequencies.

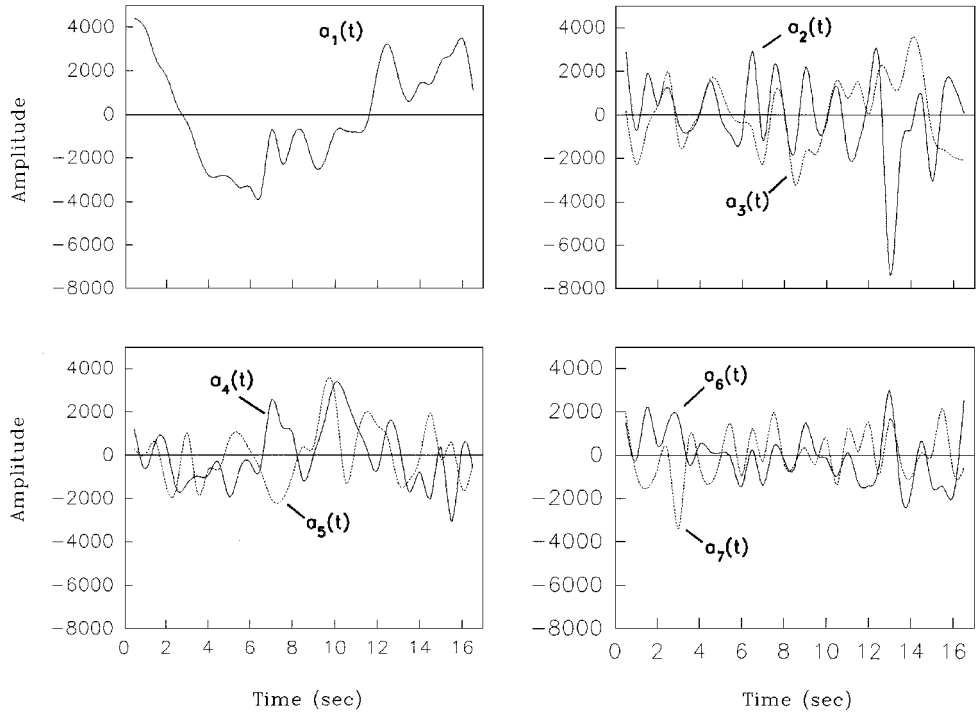

Fig. 7 Expansion coefficients for the seven most energetic modes determined by a direct projection of velocity data on the eigenfunctions.

Finally, note the large negative spike in the plot of $a_2(t)$. The time of its occurrence, $t = 13$ s, coincides with large excursions of the location of vortex breakdown observed in the experimental data between $t = 12.5$ and 14 s (Ref. 22). This implies that the second mode represents structures associated with the larger-scale streamwise fluctuations in the location of vortex breakdown. A zero crossing analysis reveals a characteristic period of 1.8 s, which is on the order of that determined for the fluctuation of the location of vortex breakdown directly from the experimental data.[22]

Overall, applying POD to this sequence of images has produced a representation that both captures the coherent structures of the flow and eliminates some of the insignificant small-scale features present in the original data. It is found that 75% of the fluctuation energy is contributed by approximately half of the eigenfunctions. Examination of the expansion coefficient $a_2(t)$ reveals similar trends between its variation with time and that observed for the fluctuations of the location of vortex breakdown in the original experimental data.

Effect of Forced Harmonic Oscillations

Proper orthogonal decomposition is applied to a sequence of images acquired in a crossflow plane as the wing undergoes harmonic oscillations in roll to demonstrate the effect of external forcing on the organization of the flow. PIV data from two complete cycles of the motion are analyzed to deduce the dominant structures and their time dependence. Each cycle has a period $T = 16.7$ s and an amplitude of 10 deg. This period of oscillation corresponds to a reduced frequency $\kappa = (\pi b)/2U_\infty T = 0.2$ and was selected, as was the delta wing geometry, to link these experiments with wind-tunnel tests at Wright Laboratory.[6] The images are obtained in 0.5-s intervals, generating 33 images per cycle. Figure 8 shows one typical instantaneous velocity field and the velocity field resulting from the ensemble average of all of the images comprising one complete cycle. The corresponding contours of constant vorticity are shown adjacent to the velocity fields. In each image, the flow is out of the page. The field of view lies in the breakdown region on the port side and in the vicinity of breakdown on the starboard side.

The analysis was performed on two separate sets of data, one containing images from one cycle, or 33 snapshots ($M = 33$), and one containing images from two cycles, or 66 snapshots ($M = 66$). A comparison of the cumulative energy distribution vs the relative mode number m/M for the two cases demonstrates that increasing the number of cycles analyzed has no significant effect on the POD analysis in terms of the distribution of energy over the modes.[22] The results of the decomposition from the 33-snapshot case (representing one motion cycle) will be the focus of the remainder of this section. In contrast to the cases considered in the preceding sections, the bulk of the energy is concentrated in the first several modes, with the first four modes containing approximately 75% of the energy in both decompositions. This high degree of concentration of energy in the lowest modes indicates a higher degree of organization of the flow structure.

Consideration of the eigenfunctions for the fluctuating component of velocity provides insight into the relative energies of flow structures of different scales. Plots of the first 5 modes and the 10th mode are presented in Fig. 9. The first eigenfunction exhibits structures of the same spatial scale as those in the averaged velocity field shown in Fig. 8b. Inspection of subsequent eigenfunctions reveals pairing in terms of the scales of the spatial structures that they represent. The fifth eigenmode, which corresponds to a normalized eigenvalue of 0.0203 (or 2.03% of the total fluctuation energy), captures significantly smaller features of the flow than the first eigenmode, which contains 62.2% of the total fluctuation energy (see Fig. 9). The 10th eigenfunction represents features of smaller scale than those in ϕ_5 and corresponds to a computed normalized eigenvalue of 0.0115. Lower-energy, higher-order modes are not retained in the truncated series expansion [Eq. (6)].

The reconstructed instantaneous velocity fields obtained using the first 10 eigenfunctions were employed to construct the three representative instantaneous sectional streamline patterns presented in Fig. 10 (left-hand column). The corresponding streamline patterns from the original PIV data are also shown (right-hand column). The close correlation of the overall topologies demonstrates that 10 eigenmodes are sufficient to create an accurate representation of the dominant flow structures. Particularly evident is the close agreement of the locations of the saddle points (apparent intersection of streamlines) at the top of each image for all values of the roll angle Φ. Images A represent the first snapshot of the sequence. Although the streamline pattern resulting from the truncated POD series is somewhat smoother than the original data, two clear limit cycles occur: unstable on the port side and stable on the starboard side, matching the topology of the original data. The streamline topologies in images B, acquired near the minimum roll angle of the cycle, also take the same fundamental form. However, the small-scale structures visible in the separating shear layers of the original data are lost. Finally, the bottom pair of images, C, show an image acquired near the maximum roll angle. The tight spiraling of the starboard

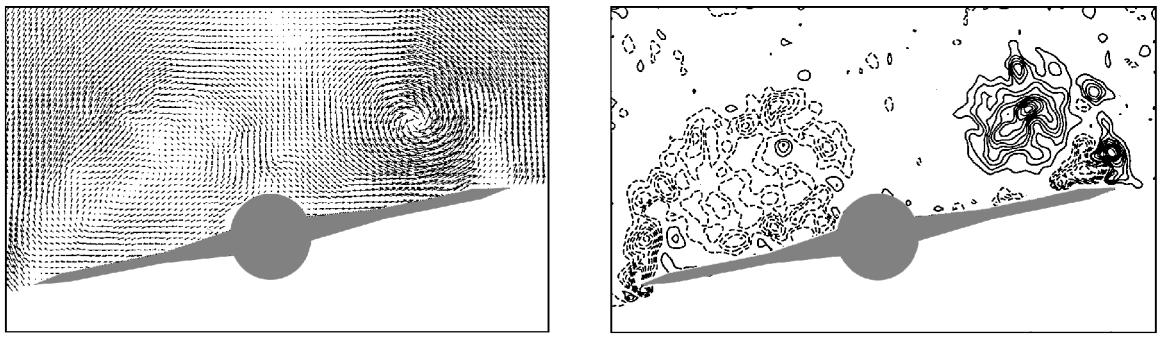

a) Instantaneous image at $\Phi = -12$ deg

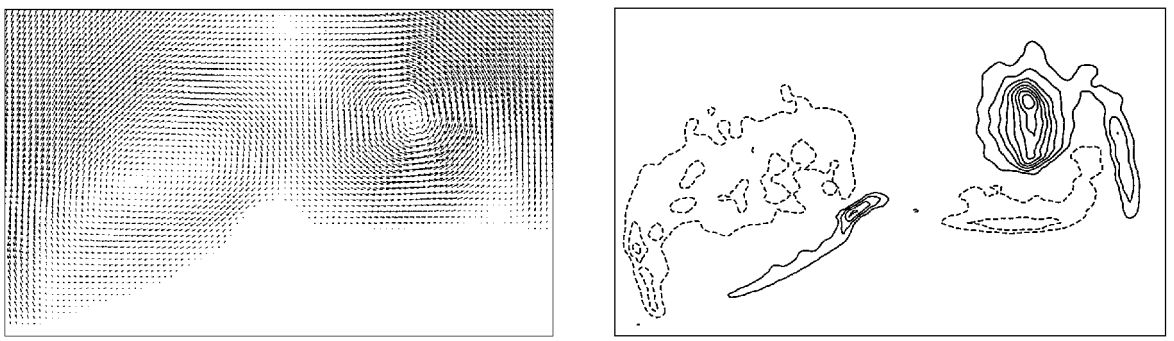

b) Average of all snapshots in one cycle

Fig. 8 Velocity fields and patterns of vorticity for forced harmonic oscillation in roll; $T = 16.7$ s, $\Phi_o = -12$ deg, and $\Delta\Phi = 10$ deg: a) typical instantaneous and b) ensemble-averaged images are shown. Minimum and incremental vorticity levels are $\omega_{\min} = \pm 5\ \mathrm{s}^{-1}$ and $\Delta\omega = 5\ \mathrm{s}^{-1}$, respectively.

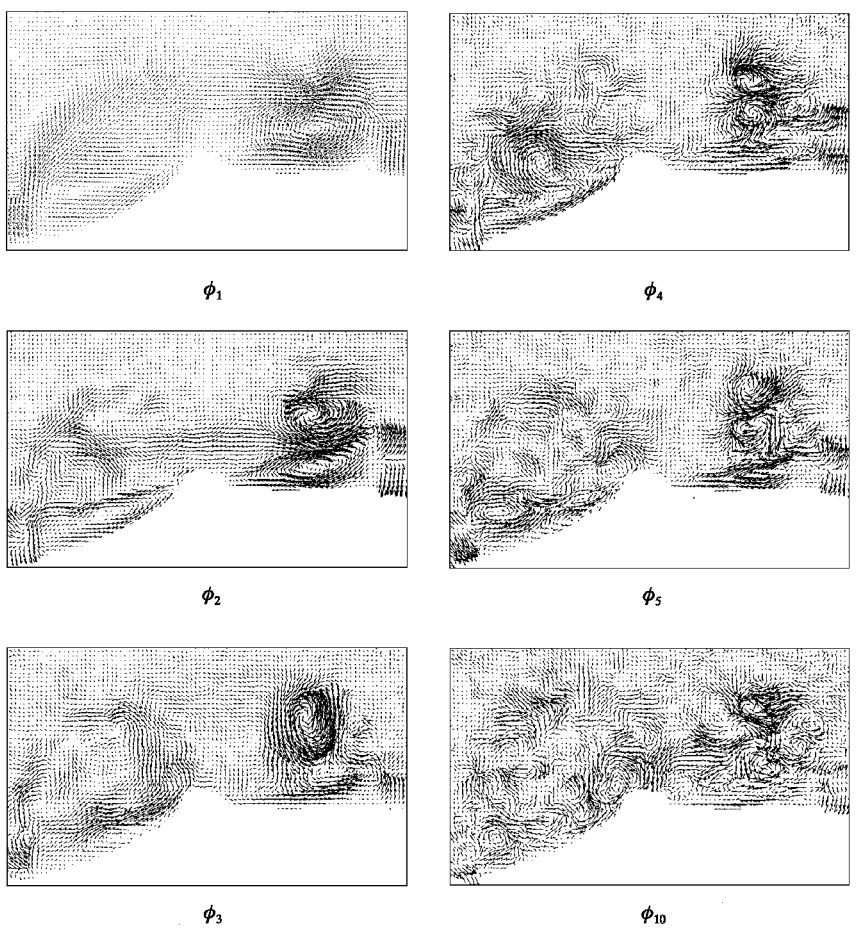

Fig. 9 Representative eigenfunctions for the case of forced harmonic oscillations; $T = 16.7$ s, $\Phi_o = -12$ deg, and $\Delta\Phi = 10$ deg.

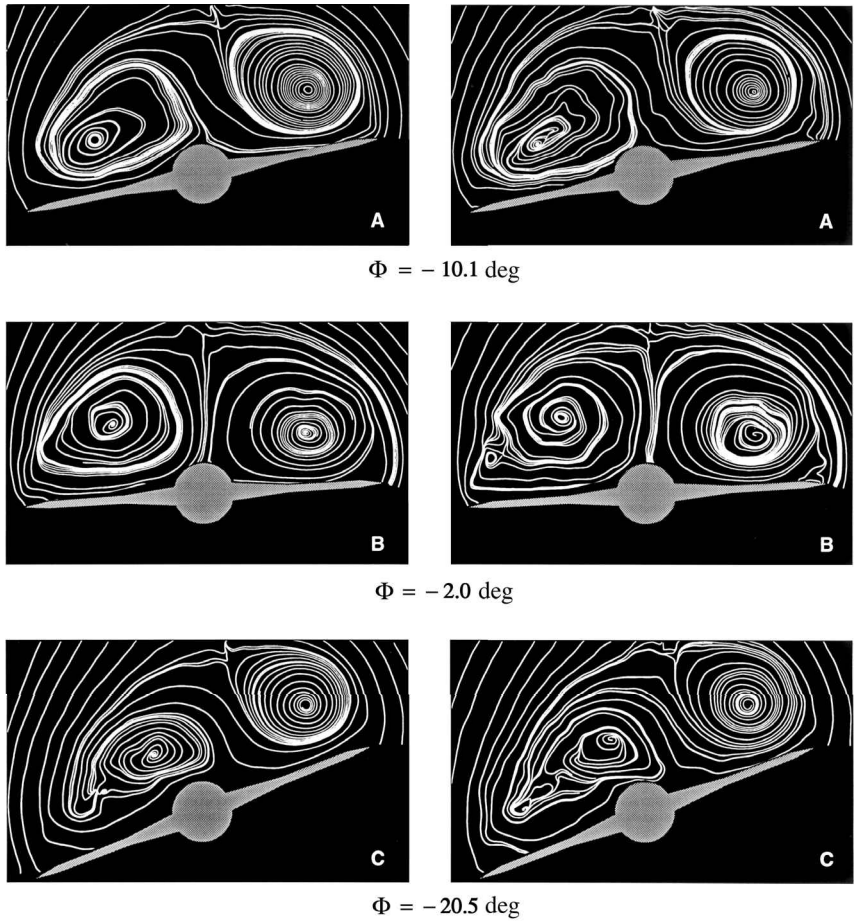

Fig. 10 Instantaneous sectional streamline patterns corresponding to reconstructed (left) and original (right) velocity fields at three selected instants during oscillation in roll.

vortex is evident, as is the unstable topology, typical of a stall region, on the port side of both images. The results in Fig. 10 demonstrate, as expected, that the reconstructed fields contain the principal large-scale structures of the original data, whereas some of the small-scale structures are smoothed out. Furthermore, the variation of the streamline topology of the flow is captured by a small number of empirical eigenfunctions, thus demonstrating the ability of POD to yield a high compression ratio without significant loss of information.

V. Concluding Remarks

The snapshot version of proper orthogonal decomposition has been applied successfully to experimental PIV measurements of flow past a delta wing and has proven to be an effective technique for identification and analysis of the coherent flow structures. The distribution of the computed eigenvalues reveals the degree of organization of the flow and the distribution of energy among the modes. For a stationary delta wing, a large number of structures of varying scales exist in the flow. In contrast, external forcing of the wing imposes a high degree of organization, and consequently, the majority of the total fluctuation flow energy is concentrated in the first few modes. Furthermore, guided by the distribution of energy among the eigenmodes, one can filter out random small-scale temporal and spatial features in the original data by retaining a limited number of modes in the reconstruction.

The computed stationary eigenfunctions represent the spatial coherent structures in the flow. The inherent timescales of the flow are reflected in the characteristic frequencies of the expansion coefficients. By appropriately combining these spatiotemporal components, the dynamical coherent structures of the flow that evolve in both space and time are identified, with the flow features of highest energy captured by the lowest-order modes.

In the present application, the largest-scale features of the leading-edge vortices can be reconstructed by including as few as two eigenfunctions in the reconstruction series. Furthermore, inclusion of half of the calculated modes produces a reconstructed field that captures the majority of the essential flow features. The use of topological concepts, based on critical point theory, to identify key features of the instantaneous structure of the leading-edge vortex has proven effective for classifying the principal features of the leading-edge vortex system.[22,26] From a practical standpoint, the ability of snapshot POD to isolate the highest-energy flow structures could have important implications to aerodynamic loading estimates, in which the largest-scale features are important. Although beyond the scope of this paper, decomposition of the flow features into discrete energy modes could allow the examination of each mode separately. This approach would enable correlation between physical flow features and specific POD modes.

In this investigation, POD has been performed on data sets consisting of 12, 33, and 66 snapshots. The spatial resolution of each snapshot was predetermined by parameters set during the PIV calculations. Subsequent studies involving the application of POD to experimental PIV data should include a rigorous examination of the effects of varying both the number of snapshots and the spatial resolution. Nonetheless, the results of the present analysis demonstrate that, for the flow considered in this work, POD can be applied effectively to even a limited number of snapshots. Finally, although the time resolution was limited by the capability of the camera used in the current set of experiments, the effect of higher time resolution should be explored in future studies.

Acknowledgments

Primary support for the work of K. M. Cipolla and D. O. Rockwell was received from the U.S. Air Force Office of Scientific Research, with supplemental support from the Office of Naval Research and the National Science Foundation. The work of A. Liakopoulos was supported by the NASA Lewis Research Center under Contract NAG3-1632.

References

[1]Hanff, E. S., and Jenkins, S. B., "Large-Amplitude High-Rate Roll Experiments on a Delta Wing and Double Delta Wing," AIAA Paper 90-0224, Jan. 1990.

[2]Hanff, E. S., and Huang, X. Z., "Roll-Induced Cross-Loads on a Delta Wing at High Incidence," AIAA Paper 91-3223, Sept. 1991.

[3]Ericsson, L. E., and Hanff, E. S., "Unique High-Alpha Roll Dynamics of a Sharp-Edged 65 Deg Delta Wing," AIAA Paper 92-0276, Jan. 1992.

[4]Ericsson, L. E., and Hanff, E. S., "Further Analysis of High-Rate Rolling Experiments of a 65 Deg Delta Wing," AIAA Paper 93-0620, Jan. 1993.

[5]Jenkins, J. E., and Myatt, J. H., "Modeling Nonlinear Aerodynamic Loads for Aircraft Stability and Control Analysis," *Stability in Aerospace Systems*, AGARD Rept. R-789, Paper 13, 1993.

[6]Jenkins, J. E., Myatt, J. H., and Hanff, E. S., "Body-Axis Rolling Motion Critical States of a 65-Degree Delta Wing," AIAA Paper 93-0621, Jan. 1993.

[7]Magness, C., Robinson, O., and Rockwell, D., "Unsteady Crossflow on a Delta Wing Using Particle Image Velocimetry," *Journal of Aircraft*, Vol. 29, No. 4, 1992, pp. 707–709.

[8]Magness, C., Robinson, O., and Rockwell, D., "Laser-Scanning Particle Image Velocimetry Applied to a Delta Wing in Transient Maneuver," *Experiments in Fluids*, Vol. 15, No. 3, 1993, pp. 159–167.

[9]Towfighi, J., and Rockwell, D., "Instantaneous Structure of Vortex Breakdown on a Delta Wing via Particle Image Velocimetry," *AIAA Journal*, Vol. 31, No. 6, 1993, pp. 1160–1162.

[10]Lin, J.-C., and Rockwell, D., "Transient Structure of Vortex Breakdown on a Delta Wing," *AIAA Journal*, Vol. 33, No. 1, 1995, pp. 6–12.

[11]Gu, W., Robinson, O., and Rockwell, D., "Control of Vortices on a Delta Wing by Leading-Edge Injection," *AIAA Journal*, Vol. 32, No. 7, 1993, pp. 1177–1186.

[12]Cipolla, K., and Rockwell, D., "Flow Structure on Stalled Delta Wing Subjected to Small-Amplitude Pitching Oscillations," *AIAA Journal*, Vol. 33, No. 7, 1995, pp. 1256–1262.

[13]Lumley, J. L., *Stochastic Tools in Turbulence*, Academic, New York, 1971, pp. 54–82.

[14]Liakopoulos, A., and Hsu, C. C., "On a Class of Compressible Laminar Boundary-Layer Flows and the Solution Behaviour Near Separation," *Journal of Fluid Mechanics*, Vol. 149, 1984, pp. 339–353.

[15]Berkooz, G., Holmes, P., and Lumley, J. L., "The Proper Orthogonal Decomposition in the Analysis of Turbulent Flow," *Annual Review of Fluid Mechanics*, Vol. 25, 1993, pp. 539–575.

[16]Liakopoulos, A., Blythe, P. A., and Gunes, H., "A Reduced Dynamical Model of Convective Flows in Tall Laterally Heated Cavities," *Proceedings of the Royal Society of London A*, Vol. 453, 1997, pp. 663–672.

[17]Moin, P., and Moser, R. D., "Characteristic-Eddy Decomposition of Turbulence in a Channel," *Journal of Fluid Mechanics*, Vol. 200, 1989, pp. 471–509.

[18]Sirovich, L., Ball, K. S., and Keefe, L. R., "Plane Waves and Structures in Turbulent Channel Flow," *Physics of Fluids A*, Vol. 2, No. 12, 1990, pp. 2217–2226.

[19]Rempfer, D., and Fasel, H. F., "Evolution of Three-Dimensional Coherent Structures in a Flat-Plate Boundary Layer," *Journal of Fluid Mechanics*, Vol. 260, 1994, pp. 351–375.

[20]Huang, H., "Limitations of and Improvements to PIV and Its Application to a Backward-Facing Step Flow," Ph.D. Dissertation, Hermann Foettinger Inst., Technical Univ. of Berlin, Berlin, Germany, 1994.

[21]Sirovich, L., "Turbulence and the Dynamics of Coherent Structures, Parts I–III," *Quarterly of Applied Mathematics*, Vol. 45, No. 3, 1987, pp. 561–590.

[22]Cipolla, K., "Structure of the Flow Past a Delta Wing with Variations in Roll Angle," Ph.D. Dissertation, Dept. of Mechanical Engineering and Mechanics, Lehigh Univ., Bethlehem, PA, June 1996.

[23]Rockwell, D. O., Magness, C., Towfighi, J., Akin, O., and Corcoran, T., "High Image-Density Particle Image Velocimetry Using Laser Scanning Techniques," *Experiments in Fluids*, Vol. 14, 1993, pp. 181–192.

[24]Seke, E., "'PIV3' Interrogation Software," Fluid Mechanics Lab., Internal Rept., Dept. of Mechanical Engineering and Mechanics, Lehigh Univ., Bethlehem, PA, 1993.

[25]Sahan, R. A., Gunes, H., and Liakopoulos, A., "Low-Dimensional Models for Coupled Momentum and Energy Transport Problems," *1995 International Mechanical Engineering Congress, Cooling and Thermal Design of Electronic Systems*, edited by C. Amon, American Society of Mechanical Engineers Press, San Francisco, CA, 1995, pp. 1–15.

[26]Magness, C., Robinson, O., and Rockwell, D. O., "Instantaneous Topology of the Unsteady Leading-Edge Vortex at High Angle of Attack," *AIAA Journal*, Vol. 31, No. 8, 1993, pp. 1384–1391.

A. Plotkin
Associate Editor